A SIMPLE WAKE-UP SCHEME BASED ON ULTRA-WIDEBAND BEAMFORMING

Florian Trösch, Frank Althaus, and Armin Wittneben

Communication Technology Laboratory, ETH Zurich, CH-8092 Zurich, Switzerland
Email: {troeschf,althaus,wittneben}@nari.ee.ethz.ch

ABSTRACT

Ultra-wideband impulse radio (UWB-IR) is a promising technology for *low-data-rate/ location-tracking* (LDR/LT) sensor networks merging low complexity system design with good localization capabilities. We consider a network with a large number of *semi-active* sensor nodes and a *static wireless backbone.* During idle times, only a low power wake-up detector is active at sensor side reducing power consumption. The wireless backbone consisting of distributed UWB-IR devices coordinates the sensor network by triggering specific nodes by means of beamforming. Sufficient conditions for principle feasibility are established and investigated as a function of the number of backbone devices. Promising performance results are shown, if the evaluated conditions are respected.

1. INTRODUCTION

Recent progresses in wireless communications and electronics enabled the development of low-cost, *low-data-rate* (LDR), multi-functional sensor networks. A typical sensor network consists of a data source or sink, such as a wireless backbone, which communicates with a sensor field containing a large, varying number of sensor nodes that are densely deployed in an area of interest. While hardware constraints on the backbone can be rather loose, constraints on sensor nodes are stringent. Their production costs should be small and often, they are equipped with very limited power sources. Hence, only simple hardware structures are suited for sensor nodes, minimizing cost, complexity, and power consumption.

Due to inherent characteristics, *ultra-wideband impulse radio* (UWB-IR) is a promising technology for *low-data-rate/ location-tracking* (LDR/LT) sensor networks [1, 2]. UWB-IR systems are intended to operate over a bandwidth of up to 7.5 GHz and are rigorously power constraint by regulations, e.g., by the *Federal Communications Commission* (FCC) [3]. The transmitters produce short time pulses without the need for additional *radio frequency* (RF) mixing stages. This leads to significant complexity reduction with respect to conventional radio systems. Furthermore, the large signal bandwidth allows for high accuracy in ranging and localization. These localization capabilities combined with the possibility to design low complexity devices, make UWB-IR a promising technology for LDR/LT sensor networks. Unfortunately, the large signal bandwidth together with the stringent power constraints increases complexity of coherent receivers, favoring non-coherent receiver design at sensor side.

Wake-up radio is a well-known network principle proposed for classic ad-hoc networks, to reduce energy consumption during idle times. As power consumption is a fundamental problem in sensor networks, we propose a similar principle for UWB-IR. The considered network consists of a large number of *semi-active* sensor nodes and a *static wireless backbone.* During idle times, sensor nodes fall into stand-by mode, and only a low power wake-up detector stays active. It has neither position nor channel state information and triggers active mode if it receives energy from the backbone corresponding to a wake-up pulse. The wireless backbone consists of cooperating devices, statically mounted on the environment around the sensor field. They are connected wirelessly or by wire to exchange global channel and positioning information and are assumed perfectly synchronized. By beamforming, the backbone steers which sensor nodes enter active mode centralizing *medium-access-control* (MAC) responsibility of the sensor field.

A temperature control system in a greenhouse is an interesting application example. The backbone beamforms to specific regions and receives temperature information, without the need for further sensor identification. Inversely, the backbone can be used to acquire location information of sensor nodes by scanning the area and waiting for responses.

In the following section, the detailed scenario and signal model of the new wake-up scheme is introduced. In Section 3, analysis of the proposed scheme is presented, followed by performance simulations in Section 4. Finally, Section 5 provides some conclusions.

2. SIGNAL MODEL

2.1. Scenario

The backbone devices are statically mounted on the wall of a circular room with equal spacing d, while sensor nodes

The authors would like to thank all partners of the PULSERS project (www.pulsers.net), that is partially funded by the European Commission and the Swiss Federal Office for Education and Science, for their contributions and constructive discussions.

are distributed over the area enclosed by the antennas, as shown in Fig. 1. No important scatterers or shadowing objects are present and therefore, *line-of-sight* (LOS) conditions dominate. This scenario is chosen for convenience, as it allows good understanding of the principle, while keeping system parameters flexible. Application of proposed wake-up scheme to any other room shape is straight forward.

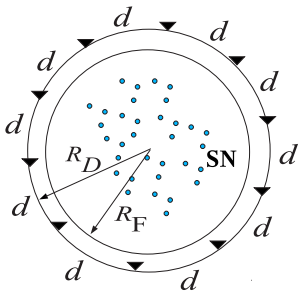

Fig. 1. Investigated scenario

2.2. Path Loss Model

Assuming a transmit pulse of uniform power spectral density, and lower and upper cut-off frequency f_l and f_u, respectively, the linear UWB-IR path loss factor is modeled as

$$\Psi_d = \left(Ad^{-\gamma}\right)^{-1} = \left(\frac{1}{B}\int_{f_\text{l}}^{f_\text{u}} \frac{c^2}{(4\pi f)^2 d^\gamma} df\right)^{-1}, \qquad (1)$$

with the bandwidth B, the speed of light $c = 3 \cdot 10^8$ m/ s and the path loss exponent γ. This model is only valid in the far-field region of a transmit antenna [4]. Hence, a minimal separation d_f between sensor nodes and transmit antennas has to be respected. Assuming a $\lambda/2$-dipole, this minimal distance equals

$$d_\text{f} = \lambda_\text{max} = \frac{c}{f_\text{min}} = 0.1 \text{ m}, \qquad (2)$$

with $f_\text{min} = 3.1$ GHz, the minimal allowed UWB frequency with respect to the FCC. According to (1), the path loss factor is often split into a frequency dependent part A and a distance dependent part $d^{-\gamma}$.

2.3. Channel Model

Due to strong LOS conditions, the *channel impulse responses* (CIR) between backbone antennas and sensors have a dominant LOS component and weak multi-path components with negligible effect on the considered wake-up scheme. Therefore, all CIRs are modeled as dirac impulses that are scaled according to the path loss. The CIR between antenna a and sensor position j is modeled as:

$$h_{a,j}(t) = \sqrt{\frac{1}{\Psi_{a,j}}}\,\delta\left(t - \tau_{a,j}\right), \qquad (3)$$

with $\Psi_{a,j}$ the linear path loss factor, and $\tau_{a,j}$ the propagation delay between antenna a and sensor position j. This unusual UWB-IR channel model was chosen because it makes analysis tractable, whereas it still allows good approximative performance and feasibility estimation for strong LOS scenarios. The presented results can be extended to more realistic UWB-IR channels, with receive energy spread over several multi-path components, by applying known signaling schemes as equalization or time-inversion schemes.

2.4. Backbone System

The cooperating backbone devices are statically placed around the area, have global location information and are synchronized to each other, i.e., they are modeled as a single multi-antenna device. To trigger a specific sensor node, the backbone introduces virtual delays at each antenna such that the pulses from the N_a antennas add up coherently at a desired sensor location. Due to the existence of accurate UWB-IR localization algorithms [1, 5, 6], beamforming accuracy of the backbone system is not a critical issue in this work. From each antenna the backbone radiates at maximally allowed pulse energy E_p, e.g., with respect to FCC. The transmit signal steered to sensor i is described by:

$$s(t,i) \quad = \quad \sqrt{E_\text{p}} \sum_{a=0}^{N_\text{a}-1} w(t - \delta_{a,i}), \qquad (4)$$

with $w(t)$ the energy normalized transmit pulse of bandwidth B and $\delta_{a,i}$ the virtual delay introduced at antenna a.

2.5. Wake-up Detector

Due to complexity reasons, the wake-up detector is designed as a non-coherent detector applying a fixed energy threshold, equal among all sensor nodes, and it has no CSI or position information. The wake-up detector periodically scans the environment by sampling a certain observation window. The observation window, which is much larger than the receive pulse width, is synchronized to the backbone. Hence, during each observation time a wake-up procedure takes place, but the detector does not know when. Such a synchronization can be achieved by a beacon synchronization as in 802.11, whereby the wake-up detector sparsely synchronizes to a beacon signal. In Fig. 2, a schematic description of the observation window at steered (left) and not steered (right) position is shown. Considering a single wake-up call, each sensor node samples the observation window several times, indicated by the crosses. The wake-up performance is dominated by the noisy sample $\hat{y}(i,j)$, which is the sample with the largest signal component $y(i,j)$ within the observation window at position j, when steering is done to position i. Hence, the exact detector performance is approximated by the performance of a detector that samples only at time instance t_j to achieve

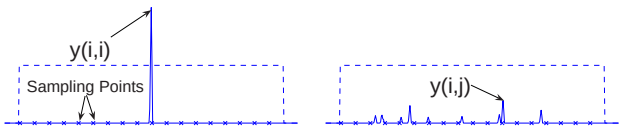

Fig. 2. Observation window at steered (left) and not steered (right) position

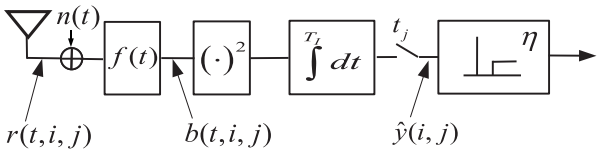

Fig. 3. Simplified signal model of wake-up detector

$\hat{y}(i,j)$. The corresponding signal model of the wake-up detector is shown in Fig. 3. The receive signal first passes an amplifier and a bandpass filter and is then squared and integrated. The integrator output is sampled at time t_j. The sensor node enters active mode, if the sample $\hat{y}(i,j)$ exceeds the threshold η.

The signal received at sensor j, when the backbone system steers to sensor position i, is given by:

$$r(t,i,j) = \sqrt{E_\mathrm{p}} \sum_{a=0}^{N_\mathrm{a}-1} h_{a,j}(t) * w(t-\delta_{a,i}) \quad (5)$$

$$= \sqrt{\frac{E_\mathrm{p}}{\Psi_{a,j}}} \sum_{a=0}^{N_\mathrm{a}-1} w(t-\tau_{a,j}-\delta_{a,i}) \quad (6)$$

with '$*$' the linear convolution. The signal $r(t,i,i)$ equals the received signal at beamed position.

Neglecting any noise contributions, i.e. $n(t) = 0$, and assuming $f(t)$ as an ideal bandpass filter of bandwidth equal to the signal component, the integrator output equals

$$y(i,j) = \frac{E_\mathrm{p}}{\Psi_{a,j}} \int_{t_j}^{t_j+T_\mathrm{I}} \left| \sum_{a=0}^{N_\mathrm{a}-1} w(t-\tau_{a,j}-\delta_{a,i}) \right|^2 dt, \quad (7)$$

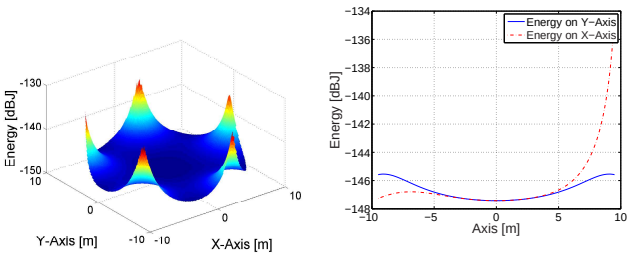

Fig. 4. (left) Energy samples $y(i,i)$ for $N_a = 5$; (right) cross sections of (left) along $y = 0$ and $x = 0$ plains

with T_I the integration duration, which is set to pulse width, i.e., $T_\mathrm{I} = 1/B$.

3. ANALYSIS

3.1. Principle Feasibility

Due to the fixed threshold at sensor side, a threshold that would allow for perfect wake-up behavior over the whole disc, neglecting noise contributions, would satisfy the following two conditions:

1: The threshold is equal or smaller than the minimal beamed energy sample, i.e.:

$$\eta \leq \eta_\mathrm{max} = \min_{\forall i} \; y(i,i). \quad (8)$$

2: The threshold is larger than the maximal non-beamed energy sample:

$$\eta > \eta_\mathrm{min} = \max_{\forall i} \left\{ \max_{\forall j \neq i} \; y(i,j) \right\}. \quad (9)$$

In principle, there is one type of non-feasible area arising from each of the two conditions. Infeasible areas arising from Condition 1, occur at positions, at which total receive energy due to path loss is small, i.e., remote from any antenna. The backbone will never be able to trigger sensor nodes in these regions. Infeasible areas arising from Condition 2, occur at positions, where energy from one antenna is dominating, i.e., in close vicinity of an antenna. Sensor nodes located within such regions always enter active mode erroneously. While both types of infeasible regions scale with the number of antennas N_a and bandwidth B, there is a clear trade-off between the two. Hence, the proposed system is designed to avoid infeasible areas arising from Condition 1 by always transmitting at maximally allowed energy and setting the threshold η equal to or smaller than the maximal feasible threshold η_max.

For the considered scenario, it can be shown by means of simple geometry that for path loss exponent $\gamma \geq 2$ and $N_\mathrm{a} \geq 5$, η_max appears at the disc center. For $\gamma \geq 2$ and $N_\mathrm{a} \leq 4$, the minimum appears not at disc center, but the energy received at disc center is close to η_max. As an example, the steered receive energy $y(i,i)$ over all positions is shown in Fig. 4 (left) for $N_\mathrm{a} = 5$, path loss exponent $\gamma = 2$, and room radius $R_\mathrm{D} = 10\,\mathrm{m}$. In order to avoid near-field considerations, the received energy is evaluated up to a radius $\tilde{R}_\mathrm{D} = R_\mathrm{D} - d_\mathrm{f} = 9.9\,\mathrm{m}$, only. Fig. 4 (right) shows two cross sections of Fig. 4 (left). The unique minima of the function is identified at disc center. Hence, η_max can be expressed as

$$\eta_\mathrm{max} = N_\mathrm{a}^2 E_\mathrm{p} A R_\mathrm{D}^{-\gamma}, \quad (10)$$

with the frequency dependent part of the path loss A according to (1) and R_D the disc radius.

We define the *infeasible region* $\mathcal{U}$ as the region in which the received pulse energy from a single antenna exceeds $\eta_{\max}$ and the *feasible region* $\mathcal{F}$ as the complementary of $\mathcal{U}$. Furthermore, we define the *feasible radius* R_{F} as the radius of the largest disc around the center which does not contain $\mathcal{U}$. While sensor nodes in $\mathcal{U}$ will always activate in the noiseless case, a sensor node in $\mathcal{F}$ can still be triggered erroneously. First, it depends on pulse bandwidth and sensor density, if neighbored nodes are triggered erroneously. Secondly, our definition of feasibility ignores unwanted constructive pulse superpositions. But antenna dominance in regions close to an antenna makes overall regions unfeasible, while constructive pulse interference occurs only on a few lines or even points for higher order superpositions. Hence, $\mathcal{F}$ and $\mathcal{U}$ are simple and meaningful measures with respect to system feasibility.

As single pulse energy is monotonically decreasing with increasing separation between sensor location and antenna, it follows that $\mathcal{U}$ can be approximated by N_{a} semi-discs around the backbone antennas. The radius R_{C} of the semi-discs is determined by the distance between a specific antenna a and the point on the connecting line between antenna a and the disc center, at which single pulse energy from antenna a equals $\eta_{\max}$. Equating single pulse energy and $\eta_{\max}$:

$$E_{\mathrm{p}} A R_{\mathrm{C}}^{-\gamma} = N_{\mathrm{a}}^2 E_{\mathrm{p}} A R_{\mathrm{D}}^{-\gamma}, \quad (11)$$

leads to:

$$R_{\mathrm{C}} = N_{\mathrm{a}}^{-2/\gamma} R_{\mathrm{D}} \quad \text{for} \quad R_{\mathrm{C}} > 0.1\ \mathrm{m}. \quad (12)$$

The total infeasible and feasible regions, $\mathcal{U}$ and $\mathcal{F}$, are:

$$\mathcal{U} = \frac{1}{2} N_{\mathrm{a}} \pi \left(N_{\mathrm{a}}^{-2/\gamma} R_{\mathrm{D}} \right)^2 \quad (13)$$

$$\mathcal{F} = \pi R_{\mathrm{D}}^2 - \mathcal{U}. \quad (14)$$

The *feasibility coverage* ($\mathrm{Cov_f}$) and the *feasibility outage* ($\mathrm{Out_f}$) express the feasible and non-feasible fractions of the disc:

$$\mathrm{Out_f} = \frac{\mathcal{U}}{\pi R_{\mathrm{D}}^2} = \frac{1}{2} N_{\mathrm{a}}^{\frac{\gamma-4}{\gamma}} \quad (15)$$

$$\mathrm{Cov_f} = 1 - \frac{1}{2} N_{\mathrm{a}}^{\frac{\gamma-4}{\gamma}}. \quad (16)$$

The feasible radius R_{F} is evaluated according to $R_{\mathrm{F}} = R_{\mathrm{D}} - R_{\mathrm{C}}$. Interestingly, the pulse bandwidth hidden in E_{p} and A cancels out in (11), and does not appear in $\mathcal{U}$, $\mathcal{F}$, and the following equations.

In Fig. 5, feasibility coverage is plotted as a function of N_{a}. Significant coverage improvement is experienced by increasing N_{a}. E.g., for $\gamma = 2$, feasibility coverage increases by more than 10%, if the number of backbone antennas is changed from $N_{\mathrm{a}} = 4$ to $N_{\mathrm{a}} = 10$ and for $\gamma = 3$, the increase in coverage from $N_{\mathrm{a}} = 10$ to $N_{\mathrm{a}} = 100$ is larger than 20%. In Fig. 6, the radius R_{C} of the infeasible semi-discs is shown for

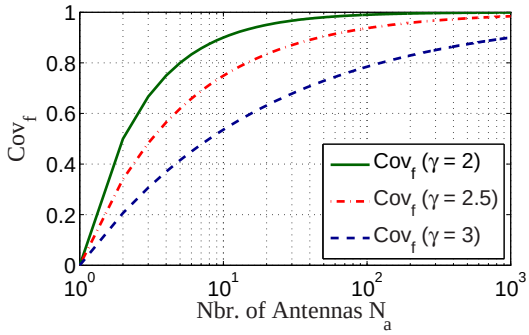

Fig. 5. Feasibility coverage as a function of N_{a} for different path loss exponents γ

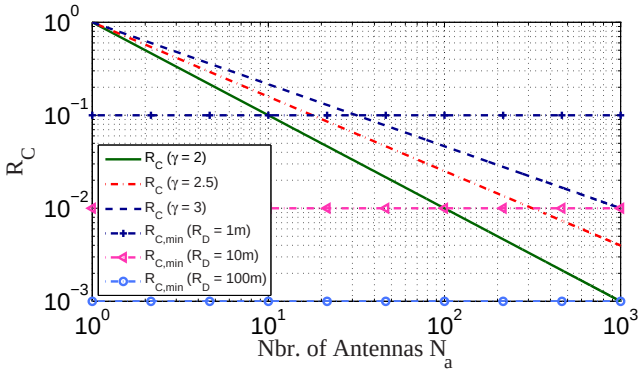

Fig. 6. Radius R_{C} for different path loss exponents γ and minimal allowed radius $R_{\mathrm{C,min}}$ for different disc radii R_{D}

different γ as a fraction of R_{D}. The minimal allowed radius $R_{\mathrm{C,min}}$ with respect to the far-field assumptions is indicated as well, for different disc radii. The cross sections determine the maximal number of backbone antennas for which conclusions are valid.

In Fig. 7, feasible and infeasible regions according to analysis are plotted for $N_{\mathrm{a}} = 4$ (left) and $N_{\mathrm{a}} = 10$ (right). It is apparent that with the presented simple threshold approach reasonable feasibility coverage is achieved. By designing a sensor network application such that a minimal distance between antennas and sensor nodes is guaranteed, well functioning systems can be expected. For example, if $N_{\mathrm{a}} = 10$ backbone antennas are applied in a room of radius $R_{\mathrm{D}} = 10$ m,

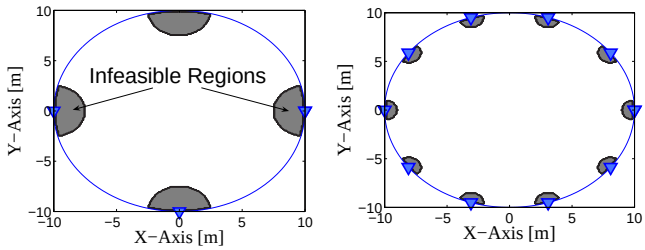

Fig. 7. Feasible coverage and outage regions for $\gamma = 2$, and $N_{\mathrm{a}} = 4$ (left) and $N_{\mathrm{a}} = 10$ (right)

a minimal separation of $R_{\text{C,min}} = 1\ \text{m}$ has to be guaranteed to design a working system. In a three dimensional realistic hall, where antennas are mounted below the roof, this seems to be no problem.

3.2. Probabilities of False Alarm and Missed Detection Within Feasible Regions

After investigation of principle feasibility, system performance is evaluated under consideration of thermal noise at the wake-up detector. While the exact *probability of false alarm* $\hat{p}_{\text{FA}}$ and *probability of missed detection* $\hat{p}_{\text{MD}}$ depend on all integrator samples within the observation window, they can be approximated by the corresponding probabilities p_{FA} and p_{MD}, which are only based on the samples $\hat{y}(i,j)$. The evaluated p_{MD} is a tight upper bound on the exact probability of missed detection, while the estimated p_{FA} gives a tight lower bound for moderate size of the observation window.

The probabilities of false alarm and missed detection given a certain room size, number of backbone antennas, and threshold, are described by:

$$p_{\text{FA}} = \sum_{\forall i} \sum_{\forall j \neq i} P(\hat{y} > \eta | i,j)\ P(i,j) \tag{17}$$

and

$$p_{\text{MD}} = \sum_{\forall i} P(\hat{y} \leq \eta | i,i)\ P(i,i), \tag{18}$$

with $P(i,j) = \frac{1}{N(N-1)}$, $P(i,i) = \frac{1}{N}$, and N, the total number of sensor positions considered.

Due to the property that the integration duration equals pulse width, i.e., $T_{\text{I}} = T_{\text{p}}$, the scheme in Fig. 3 can be modeled as a non-coherent one tap receiver. Hence, the receive signal at the j-th sensor, when steering is done to position i, can be modeled as:

$$r(i,j) = \sqrt{y(i,j)}, \tag{19}$$

whereby $y(i,j)$ represents $\hat{y}(i,j)$ in the noiseless case. The signal $b(i,j)$ after the bandpass filter equals:

$$b(i,j) = \sqrt{y(i,j)} + \tilde{n}, \tag{20}$$

with $\tilde{n}$ a zero-mean complex Gaussian random variable of variance $\sigma^2 = 2N_{\text{E}}$. The conditional probabilities of false alarm and missed detection are now given by

$$P\left(\hat{y} > \eta | i,j\right) = P\left(|b|^2 > \eta | i,j\right), \tag{21}$$

and

$$P\left(\hat{y} \leq \eta | i,i\right) = P\left(|b|^2 \leq \eta | i,i\right), \tag{22}$$

Substituting $Z = |b(i,j)|^2$ leads to a non-central chi-square random variable with two degrees of freedom [7]:

$$p_Z(z) = \frac{1}{2\sigma_n^2} e^{-(s^2+z)/2\sigma_n^2} I_0\left(\sqrt{z}\frac{s}{\sigma_n^2}\right) \tag{23}$$

with I_0 the 0-th order modified Bessel function of the first kind, $s = \sqrt{\hat{y}(i,j)}$, and $\sigma_n^2 = \sigma^2/2$. Expressing the *cumulative distribution function* (CDF) of z in terms of the first order generalized Marcum's Q-function yields [7]:

$$F_Z(z) = 1 - Q_1\left(\frac{s}{\sigma_n}, \frac{\sqrt{z}}{\sigma_n}\right). \tag{24}$$

Finally, we have the following results on the conditional probabilities:

$$P\left(\hat{y} > \eta | i,j\right) = Q_1\left(\sqrt{y(i,j)/N_{\text{E}}}, \sqrt{\eta/N_{\text{E}}}\right) \tag{25}$$

$$P\left(\hat{y} \leq \eta | i,i\right) = 1 - Q_1\left(\sqrt{y(i,i)/N_{\text{E}}}, \sqrt{\eta/N_{\text{E}}}\right). \tag{26}$$

4. SIMULATION RESULTS

4.1. Feasible Regions Neglecting Thermal Noise

As we assume high beamform accuracy, minimal resolvable separation d_{min}, i.e., minimal separation between sensor nodes which can still be triggered individually, is limited by the simple detector. It is mainly determined by the receive pulse width in time domain $T_{\text{p}} = 1/B$ leading to $d_{\text{min}} \approx cT_{\text{p}}$. If the sensors are located closer than d_{min}, the presented threshold approach does not work properly. E.g., for a pulse bandwidth of $B = 500\ \text{MHz}$, resolvable sensor nodes have to lie at least $60\ \text{cm}$ apart from each other. To achieve accurate resolvability in a sensor network where sensors are placed on a two dimensional rectangular grid of $10\ \text{cm}$, an approximate pulse bandwidth of $3\ \text{GHz}$ is required.

To confirm intuition, a beam pattern over the whole disc is plotted in Fig. 8, for steering position $(x_0, y_0) = (-1, -1)\,\text{m}$, i.e., $y(i,j),\ \forall j$ are plotted for a specific i. The plot is scaled in dBJ, pulse bandwidth is set to $3\ \text{GHz}$, number of antennas equals $N_{\text{a}} = 10$, and path loss exponent is $\gamma = 2$. The disc radius equals $3\ \text{m}$ and spatial sampling was done on a cartesian two dimensional grid of $10\ \text{cm}$. The antenna positions can be identified at the edge of the disc. The width of the beamed pulse approximately concentrates on one spatial sample. Hence, the minimal resolvable distance between neighbored sensor nodes is indeed $10\ \text{cm}$. Respecting the minimal sensor separation $d_{\text{min}} = 10\ \text{cm}$ acceptable wake-up performance can be expected.

This intuition is confirmed by Fig. 9, which shows all beamed samples, i.e., $y(i,i),\ \forall i$ as '$\circ$' points and all non-beamed samples, i.e., $y(i,j)\ \forall i$ and $\forall j \backslash i$ as '$\times$' points, plotted over disc radius. The plot can be considered as the collection of $y(i,j)$ over all possible steering positions i and all polar coordinates ϕ from 0 to 2π. The maximal feasible threshold η_{max} is indicated, too. Within the feasible region, i.e., up to a radius of $2.7\ \text{m}$, significant energy differences between beamed and non-beamed samples can be identified, which leads to reasonable performance even under noise considerations, as we will see in the next section.

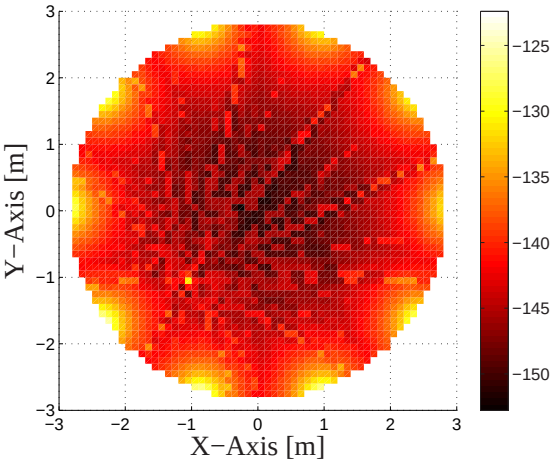

Fig. 8. Beam pattern $y(i,j)$ [dBJ] over disc, if beamforming is done to position $(x_0, y_0) = (-1, -1)$ m; for $N_\mathrm{a} = 10$, $B = 3$ GHz, and $\gamma = 2$.

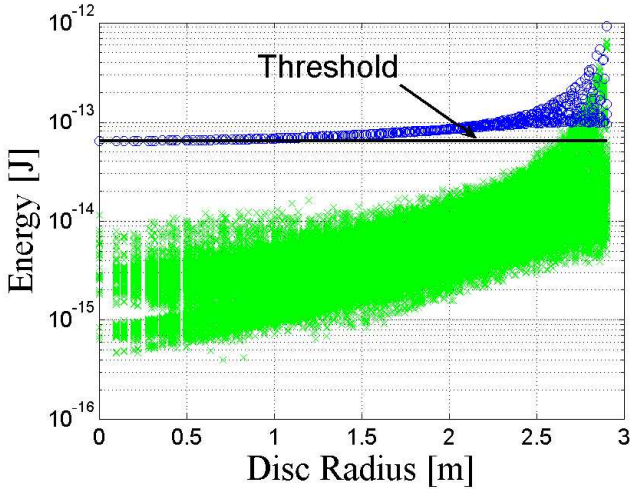

Fig. 9. All beamed samples, i.e., $y(i,i)$, $\forall i$ ($\circ$) and all non-beamed samples, i.e., $y(i,j)$, $\forall i$ and $\forall j \backslash i$ ($\times$) plotted over disc radius; for $N_\mathrm{a} = 10$, $B = 3$ GHz, and $\gamma = 2$.

Note that in Fig. 8, lines where two pulses interfere constructively are clearly identifiable. Collected energy on these lines is up to 10 dBJ larger than the energy collected in the surrounding. Hence, interfering pulses certainly have an impact on the overall wake-up performance. But from Fig. 9, it is noticeable that for reasonable design parameters, superpositions have only minor effects on the principle feasibility of the system.

4.2. Performance Within Feasible Regions

To simulate the wake-up performance within the feasible region, considering thermal noise at sensor side, we define the *signal-to-noise ratio* (SNR) without path loss:

$$\zeta = \frac{E_p}{N_\mathrm{E}}, \tag{27}$$

and the threshold η as a fraction of the maximal receive energy at disc center:

$$\eta = \tilde{\eta}\eta_\mathrm{max} = \tilde{\eta} N_\mathrm{a}^2 E_\mathrm{p} / \Psi_{\mathrm{R_D}}, \tag{28}$$

with $\tilde{\eta}$ the fractional threshold. Hence, (25) and (26) result in

$$P\left(\hat{y} > \eta | i,j\right) = Q_1\left(\sqrt{\zeta m(i,j)}, \sqrt{\tilde{\eta} N_\mathrm{a}^2 / \Psi_{\mathrm{R_D}} \zeta}\right) \tag{29}$$

$$P\left(\hat{y} \leq \eta | i,i\right) = 1 - Q_1\left(\sqrt{\zeta m(i,i)}, \sqrt{\tilde{\eta} N_\mathrm{a}^2 / \Psi_{\mathrm{R_D}} \zeta}\right), \tag{30}$$

where we used the abbreviation $m(i,j) = \frac{y(i,j)}{E_\mathrm{p}}$.

There are two major reasons to define the SNR as the ratio between transmit pulse energy from a single antenna over equivalent noise N_E at sensor node. First, normalization to receive $\mathrm{SNR_{Rx}}$ would cancel out performance gains due to increased receive power. Hence, significant gains due to increased number of antennas (devices) would be neglected. Secondly, $\mathrm{SNR_{Rx}}$ varies over the disc, while the considered SNR is a global measure.

To provide better intuition about the proposed normalization, a link budged example for the simulated scenario is established. According to [8, 9], the maximally allowed single pulse spectral energy for LDR systems in peak power regime equals $E_0 = 8.1 \cdot 10^{-20} \frac{\mathrm{W}}{\mathrm{Hz}^2}$. As the wake-up procedure happens sparsely in time, the wake-up signal is considered as LDR. Hence, single pulse energy is set to $E_\mathrm{p} = E_0 B$. The equivalent noise is defined as $N_\mathrm{E} = N_0 G_\mathrm{Amp} L_\mathrm{Ant} L_\mathrm{Imp}$, with the noise figure G_Amp, the antenna mismatch L_Ant, the implementation loss L_Imp, and $N_0 = -174 \frac{\mathrm{dBm}}{\mathrm{Hz}}$, the power spectral density of the thermal noise. Further simulation parameters are the disc radius $R_\mathrm{D} = 100$ m, the number of antennas $N_\mathrm{a} = 10$, the path loss exponent $\gamma = 2$, and the pulse frequency band from $f_\mathrm{l} = 3.1$ GHz to $f_\mathrm{u} = 6.1$ GHz. Assuming $G_\mathrm{Amp} = 17$ dB, $L_\mathrm{Ant} = 3$ dB, $L_\mathrm{Imp} = 3$ dB, the equivalent noise becomes $N_\mathrm{E} = -181\,\mathrm{W/Hz}$ and the transmit pulse energy is $E_\mathrm{p} = -96$dBJ. The path loss at 100m is $PL = 85$dB. Hence, according to

$$\mathrm{SNR}^\mathrm{c}_\mathrm{Rx} = 20 \log_{10} N_\mathrm{a} + E_\mathrm{p} - PL - N_\mathrm{E}\ [\mathrm{dB}], \tag{31}$$

$\zeta = 85$ dB corresponds to receive $\mathrm{SNR}^\mathrm{c}_\mathrm{Rx} = 20$ dB at disc center. As $G_\mathrm{Amp} = 17$ dB is a rather pessimistic noise figure, a SNR of at least 85 dB is realistic. Furthermore, $\mathrm{SNR}^\mathrm{c}_\mathrm{Rx} = 20$ dB is the smallest receive $\mathrm{SNR_{Rx}}$ over the whole disc and hence, a reasonable $\mathrm{SNR_{Rx}}$ is provided over the whole disc.

In Fig. 10 and 11, probabilities of false alarm and missed detection are shown for a fractional threshold $\tilde{\eta} = 0.7$ and $\tilde{\eta} = 0.9$, respectively. Only sensor positions within the feasi-

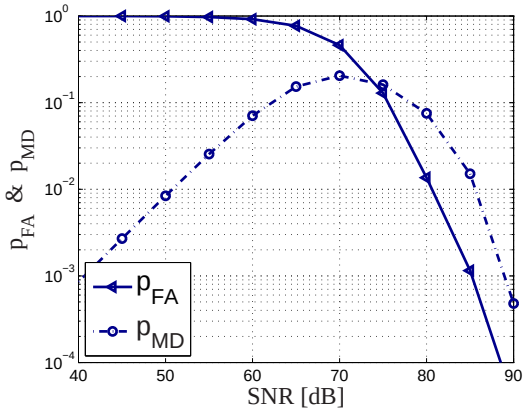

Fig. 10. Probability of false alarm and missed detection for $R_{\mathrm{D}} = 100\,\mathrm{m}$, $N_{\mathrm{a}} = 10$, $B = 3\,\mathrm{GHz}$, $\gamma = 2$, and $\tilde{\eta} = 0.7$.

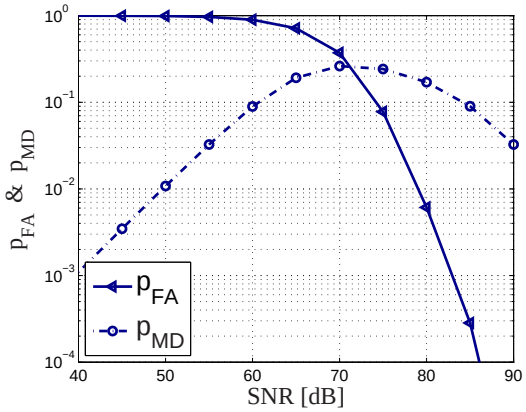

Fig. 11. Probability of false alarm and missed detection for $R_{\mathrm{D}} = 100\,\mathrm{m}$, $N_{\mathrm{a}} = 10$, $B = 3\,\mathrm{GHz}$, $\gamma = 2$, and $\tilde{\eta} = 0.9$.

ble radius R_{F}, now evaluated according to the specific chosen threshold $\eta = \tilde{\eta}\eta_{\max} \leq \eta_{\max}$, are considered for evaluation of p_{FA} and p_{MD}.

As the wake-up detector is sensitive to energy, any noise contributions increase the probability of false alarm and decrease the probability of missed detection. Hence, the probability of missed detection p_{MD} is low not only at high SNR but also at low SNR.

It can be observed that with increasing $\tilde{\eta}$ the probability of missed detection grows, i.e., at high SNR, p_{MD} is much higher in Fig. 11 than in Fig. 10, while the probability of false alarm does hardly change. This arises from the fact that the considered feasible radius R_{F} changes as a function of $\tilde{\eta}$. If $\tilde{\eta}$ would be increased while keeping the radius R_{F} constant, the probability of false alarm would improve. Hence, the improvement of p_{FA} is transformed into larger feasibility radius R_{F}, which are $R_{\mathrm{F}} = 85\,\mathrm{m}$ and $R_{\mathrm{F}} = 90\,\mathrm{m}$, respectively.

From Fig. 11, it is apparent that the threshold $\eta = \eta_{\max}$ would lead to a disastrous probability of missed detection, and hence, feasibility coverage discussed in Section 3.1 are not perfectly achievable, if thermal noise is taken into account.

5. CONCLUSIONS

A new, very simple wake-up detection scheme for strong LOS scenarios is proposed. It significantly reduces power consumption at sensor side at the expense of increased complexity and power consumption at the wireless backbone. The presented non-coherent wake-up detector requires neither CSI nor any location information at sensor node. Based on a simplified system model, sufficient conditions for principle feasibility are established and investigated as a function of the number of backbone devices. It is shown that principle feasibility strongly depends on the number of backbone devices, while pulse bandwidth has only marginal impact. Promising performance results are presented, if the evaluated conditions are satisfied.

6. REFERENCES

[1] F. Nekoogar, F. Dowla, and S. Alex, "Self organization of wireless sensor networks using ultra-wideband radios," in *IEEE Conf. Rad. and Wirel. (RAWCON)*, Atlanta, GA, Sept. 19–22, 2004, pp. 451–454.

[2] I. Oppermann, L. Stoica, A. Rabbachin, Z. Shelby, and J. Haapola, "UWB wireless sensor networks: UWEN - A practical example," *IEEE Commun. Mag.*, vol. 42, no. 12, pp. 27–32, Dec. 2004.

[3] FCC, "Revision of part 15 of the commission's rules regarding ultra-wideband transmission systems," *First Report and Order, ET-Docket 98-153, FCC 02-28*, adopted/released Sept. 19, 2005/Apr. 22, 2002.

[4] T. S. Rappaport, *Wireless Communications – Principles and Practice*, 2nd ed. Prentice Hall, 2002.

[5] B. Q. Ruiz, A. A. Vazquez, M. L. Rubio, and G. J. Garcia, "Impulse radio UWB system architecture for smart wireless sensor networks," in *Int. Workshop on Netw. with UWB and Workshop on UWB Sensor Netw. (NEUWB)*, July, 4–6, 2005, pp. 35–39.

[6] K. Yu and I. Oppermann, "UWB positioning for wireless embedded networks," in *IEEE Conf. Rad. and Wirel. (RAWCON)*, Atlanta, GA, Sept. 19–22, 2004, pp. 459–462.

[7] J. G. Proakis, *Digital Communications*, 1st ed. John Wiley & Sons, 2002.

[8] F. Trösch, F. Althaus, and A. Wittneben, "Modified pulse repetition coding boosting energy detector performance in low data rate systems," in *IEEE Int. Conf. Ultra-Wideband (ICU)*, Zurich, Switzerland, Sept. 5 – 8, 2005.

[9] ——, "Pulse position pre-coding exploiting UWB power constraints," in *IEEE Proc. SPAWC*, New York, NY, Jun. 5–8, 2005.